Nanoporous Silicon Waveguides for Biosensing

Anqi Fu, S.-Z. Lo, P. Apiratikul, A. Giovannozzi, T. E. Murphy

***Abstract*—We describe the design, fabrication, and measurement of integrated optical waveguides comprised of nanoporous silicon. A flexible direct-write scanning laser system was constructed and programed, which allows the generation of waveguides of almost any prescribed shape. We successfully wrote and measured single mode optical waveguides with both straight and curved geometries. This system lays the foundation for a new class of waveguide-based biosensors that uses on-chip integrated interferometers.**

***Index Terms*—porous silicon, optical waveguide, interferometer, biosensor**

I. Introduction

NANOPOROUS silicon is an attractive material for optical biosensing applications due to its high surface area to volume ratio, simple fabrication, and nanometer-scale features that can be fine tuned over a wide porosity range. The refractive index of the material scales in a known way with its porosity, allowing for the formation of multilayer slab waveguides. Label-free biodetection is then possible by conjugating molecules to the porous silicon surface and observing a change in optical properties through interferometry.

The total insertion loss of these structures is related both to the input and output coupling efficiency, as well as the propagation loss distributed over the length of the waveguide. Several factors contribute to the propagation loss, including the intrinsic material absorption, scattering from inhomogeneities in the waveguide boundaries, leakage of light into the high index cladding layers, and bending loss where the waveguides follow a curved path. In this study, we characterize the insertion loss of linear and bent guided wave structures, and observe the mode of the output beam via infrared imaging.

II. Previous Work

Optical sensors have had a long history, from fiberoptic gyroscopes to surface plasmon detectors. Their small size, high sensitivity, and resilience in hostile environments give them a distinct advantage over traditional electronic sensors. With the advent of integrated circuit technology, silicon in particular has attracted a great deal of interest as a material for biosensing.

The development of porous silicon can be traced back to the 1950s, when it was first produced by electrochemical etching at Bell Labs [1]. Because the pore size is small compared to the optical wavelength, nanoporous silicon behaves like an effective optical medium with a refractive index that depends on the degree of porosity [2]. The porosity, and hence the refractive index, can be adjusted over a wide range ($n_{air} < n_{eff} < n_{Si}$) by controlling the dopant concentration [3] and current density used when etching the sample [4], [5]. One of the truly unique properties of porous silicon is that the porosity can be controlled on a layer-by-layer basis – by varying the current density in time, it is possible to sequentially form complex multilayer structures (Fig. 1). This feature allows one to fabricate a high-index core layer surrounded by lower-index cladding layers, comprising a slab optical waveguide. Losses of as low as 1 dB/cm have been reported for linear structures [6].

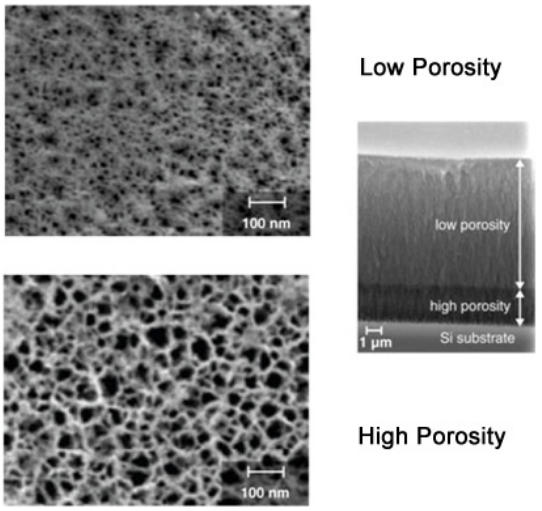

Figure 1. SEM micrograph of multilayer porous silicon structure. The porosity of each layer is directly related to the applied current density during etching.

The high internal surface area of porous silicon makes it a versatile platform for biological and chemical detection. Large numbers of molecules can be immobilized in its pores by bioconjugation [7], and changes in its optical properties observed. Measurements of loss, birefringence, and refractive index changes have been effective in detecting organic solvent vapors [8]. Recent successes with porous silicon films have demonstrated its viability as a biomolecular sensor [9], spurring research into more complex waveguide designs, such as the Mach-Zehnder interferometer.

III. Methodology

Porous silicon was prepared by electrochemical anodization of polished, p+ doped crystallined silicon wafers with resistivity of roughly 0.5-1.0 mΩ-cm. The wafer was pressed against the 1.3 cm diameter opening of a cylindrical PVC cell containing an electrolyte solution of HF:water:ethanol = 1:1:2 and a platinum sheet cathode. Etching was performed by application of current pulses via a programmable galvanostat, with anodization taking place in 0.2 sec substeps, each followed by a 10 sec etch stop to replenish the solution inside the pores. The porous silicon layers were formed by applying 440 mA/cm^2 for 4 sec, followed by 418 mA/cm^2 for the same duration, and 440 mA/cm^2 again for 27 sec. The final

slab waveguide structure (Fig. 2) exhibits a 3.8 μm thick core of 75% porosity, and 1.18 μm thick top, 8 μm thick bottom cladding of 77% porosity, with light confined by total internal reflection at the interfaces.

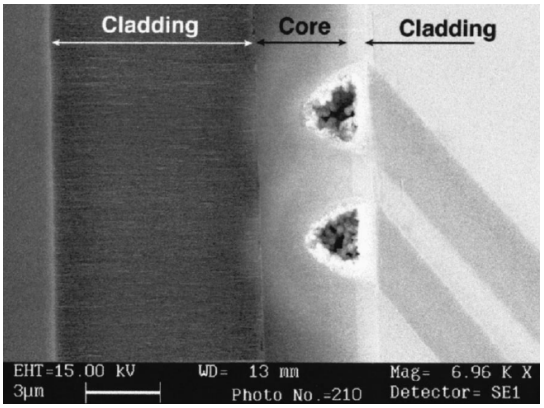

Figure 2. SEM cross-section of a PS waveguide after laser local oxidation [10]

The sample was then mounted on a motorized XY stage and a 473 nm diode-pumped solid state laser focused on its surface through a polarizing beam splitter and 40× infinity-corrected objective with a numerical aperture of 0.66 (Fig. 3). In order to provide real-time imaging during writing, a CCD camera was attached on top of the microscope zoom assembly, with co-axial illumination furnished from a collimated fiber light source. Lateral definition of the waveguide was obtained via local oxidation of lithographic strips [10] at a laser power of ~60 mW after the lens. Complex patterns may be achieved by programming the movement of the stage beneath the focused beam, thus changing the direction of the oxide paths. For the purposes of this experiment, we used a constant speed of 500 μm/s to ensure uniformity across the sample. The resulting oxide strips were etched away in dilute HF solution, leaving wells in the porous silicon that effectively confine light in the lateral direction, and RTA was performed on the entire surface at 400° C for 5 mins.

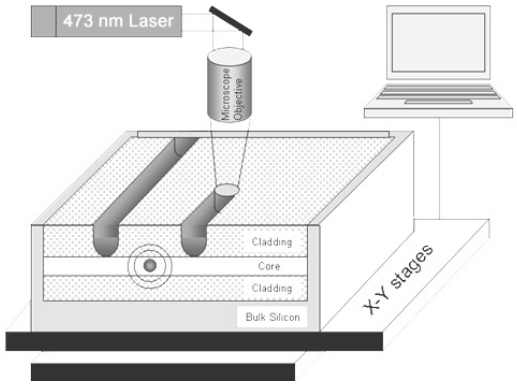

Figure 3. Laser writing setup. The beam is diverted through a periscope assembly into the laser injection port and polarizing beam splitter (not shown) before being focused through the microscope objective.

The waveguides were characterized by coupling two monomodal fibers at the cleaved edges and measuring transmission at 1550 nm for an input power of 1.4 mW. An infrared camera was employed to provide imaging of the output light. Near-field measurements were also obtained at steps of 1 μm over the distribution of the beam.

IV. Results

In the initial experiments, we fabricated straight waveguides by inscribing two parallel lines with a center-to-center spacing of 10, 15, and 20 μm. The distance between adjacent waveguides was at minimum 300 μm, to ensure no crosstalk between neighboring devices (Fig. 4a). Total insertion loss measured through the fibers was approximately -22 dB, with the highest output power 8 μW observed from the 20 μm waveguide. This includes both the coupling loss, as well as the propagation loss due to scattering at the core-cladding interfaces and material absorption. Variation of the input wavelength from 1550 to 1650 nm did not significantly alter the results. The near-field intensity distribution of the output beam (Fig. 5), taken over a 20 x 20 μm^2 area, revealed a single mode propagation along the waveguide. As the input fiber moved across the width of the waveguide, the output beam increased and decreased in intensity, but always retained its single lobe shape. Infrared photography of the elliptical spot (Fig. 6) confirmed these measurements.

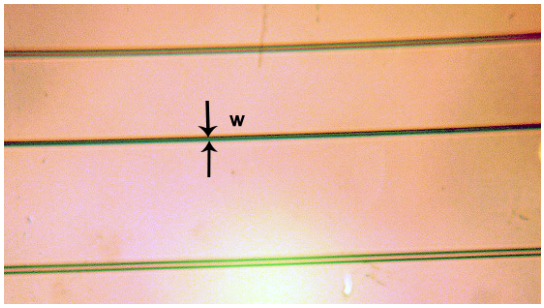

a)

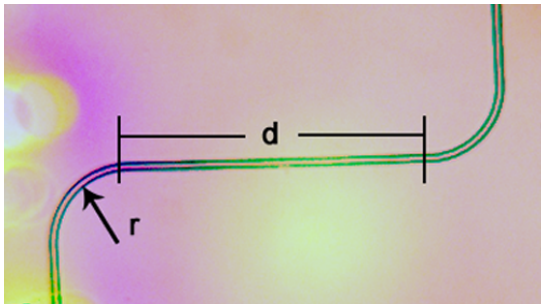

b)

Figure 4. a) Linear waveguides with w = 15, 10, and 20 μm from top down, and b) Bent waveguide with r = 250 μm, d = 0.5 mm.

Bent 90° S-shaped waveguides were fabricated with radius of curvature 250 μm and displacements 0.5 and 1.0 mm (Fig. 4b). Transmission measurements showed a high degree of insertion loss from both structures, with output power fluctuating in the nW range. Optical microscopy furthermore revealed flaws in the local oxidation pattern, specifically, oxide dots where the motorized stage paused at the beginning and end of a curve shape, and unintended tapering at the edges of the chip where the laser scanned across a cleave. These,

coupled with losses at the bends of the waveguide, prevented enough light to be collected at the output for meaningful measurements. Further investigation into the exact nature of the bending loss is required before a more suitable guiding structure can be constructed.

V. Discussion

The single mode propagation pattern presents promising groundwork for the design of an interferometric device. Aside from reducing dispersion, these waveguides are completely absorbing of the opposite polarization state, a necessary component to a Mach-Zehnder interferometer in order to maintain one phase delay within each arm so that the relative shift can be easily traced back from interference peaks at the output.

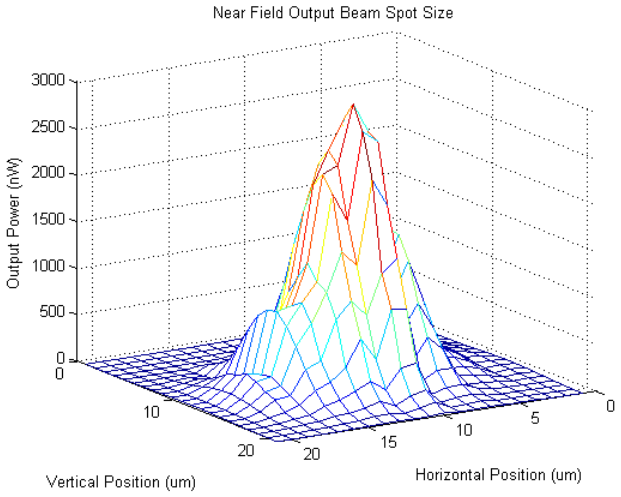

Figure 5. Spatial distribution of light intensity from 20 μm linear waveguide.

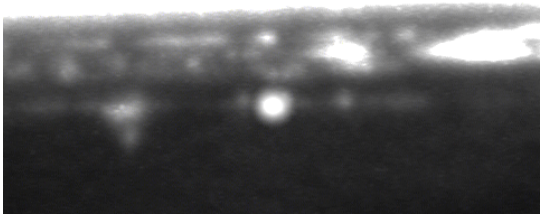

Figure 6. Infrared image of single mode output beam.

On the other hand, the insertion loss, while still adequate for the performance of some devices, could be improved. Flaws in the porous silicon itself occasionally intruded on the waveguide paths, causing scattering, and the laser drifted out of focus at times over the uneven surface, leading to non-uniform oxidation of the strips. Uneven cleaving of the wafer was seen at the edges as well, and may contribute further to coupling loss. The insertion loss could be mitigated by modifying the fabrication parameters of the porous silicon to better match the optical fiber dimensions. Lowering the dopant concentration may also reduce absorption in the material. Additionally, since the overall loss decreased with increasing distance between the oxide strips, wider waveguides of > 20 μm may exhibit even better transmission, a possible direction for future research.

In the bent structures, light leakage at the curves could be addressed by experimenting with a larger radius of curvature and smaller angle, more closely mimicking linear paths. Once functioning waveguides are fabricated, it will be possible to compare the linear and S-shapes, and calculate separately the coupling, bending and propagation loss by taking the difference of the output power. With these parameters in mind, we may begin to realize the Mach-Zehnder interferometer.

VI. Conclusion

The goal of this project is to explore the potential of porous silicon as a platform for biosensing. In that vein, a laser scanning system was designed, built, and programmed to lithographically define both linear and curved paths via laser local oxidation. Single mode waveguides were fabricated, and their insertion loss characterized using fiber-coupling techniques. Future work will focus on determing the optimal parameters to minimize bending and scattering loss, constructing a Mach-Zehnder interferometer, and functionalizing it with biomolecules to evaluate its performance as a sensor.

References

[1] A. Uhlir, "Electrolytic shaping of germanium and silicon," *Bell System Tech. J.*, vol. 35, pp. 333–347, 1956.

[2] M. G. Berger, C. Dieker, M. Thonissen, L. Vescan, H. Luth, H. Munder, W. Theiβ, M. Wernke, and P. Grosse, "Porosity superlattices: A new class of Si heterostructures," *J. Appl. Phys.*, vol. 27, p. 1333, 1994.

[3] M. Takahashi and N. Koshida, "Fabrication and characteristics of three-dimensionally buried porous silicon optical waveguides," *J. Appl. Phys.*, vol. 86, p. 5274, 1999.

[4] A. Loni, L. T. Chanam, M. G. Berger, R. Arens-Fisher, H. Munder, H. Luth, H. F. Arrand, and T. M. Benson, "Porous silicon multilayer optical waveguides," *Thin Solid Films*, vol. 276, pp. 143–146, 1996.

[5] H. F. Arrand, T. M. Benson, P. Sewell, A. Loni, R. J. Bozeat, R. Arens-Fisher, M. G. Kruger, M. Thonissen, and H. Luth, "The application of porous silicon to optical waveguiding technology," *IEEE J. Sel. Top. in Quantum Electron.*, vol. 4, pp. 975–982, 1998.

[6] N. Vorozov, L. Dolgyi, V. Yakovtseva, V. Bondarenko, M. Balucani, G. Lamedica, A. Ferrari, G. Vitrant, J. E. Broquin, T. M. Benson, H. F. Arrand, and P. Sewell, "Self-aligned oxidised porous silicon optical waveguides with reduced loss," *Electron. Lett.*, vol. 36, pp. 722–723, 2000.

[7] F. P. Mathew and E. C. Alocilja, "Porous silicon-based biosensor for pathogen detection," *Biosens. Bioelectron.*, vol. 20, pp. 1656–1661, 2005.

[8] P. A. Snow, E. K. Squire, P. S. J. Russell, and L. T. Canham, "Vapor sensing using the optical properties of porous silicon Bragg mirrors," *J. Appl. Phys.*, vol. 86, pp. 1781–1784, 1999.

[9] A. M. Rossi, L. Wang, V. Reipa, and T. E. Murphy, "Porous silicon biosensor for detection of viruses," *Biosens. Bioelectron.*, vol. 23, pp. 741–745, 2007.

[10] A. M. Rossi, G. Amato, V. Camarchia, L. Boarino, and S. Borini, "High quality porous silicon buried waveguides," *Appl. Phys. Lett.*, vol. 78, pp. 3003–3005, 2001.